Magneto-structural study of a Cr-doped $CaRuO_3$

2009 J. Phys.: Condens. Matter 21 326001

(http://iopscience.iop.org/0953-8984/21/32/326001)

J. Phys.: Condens. Matter **21** (2009) 326001 (6pp) doi:10.1088/0953-8984/21/32/326001

Magneto-structural study of a Cr-doped $CaRuO_3$

Rajeev Ranjan[1], Rohini Garg[1], Anatoliy Senyshyn[2], M S Hegde[3], Helmut Ehrenberg[4] and Hans Boysen[5]

[1] Department of Materials Science, Indian Institute of Science, Bangalore 560012, India
[2] Institute for Materials Science, Darmstadt University of Technology, Petersenstrasse 23, D-64287 Darmstadt, Germany
[3] Solid State and Structural Chemistry Unit, Indian Institute of Science, Bangalore 560012, India
[4] Institute for Complex Materials, IFW Dresden, Helmholtzstraße 20, D-01069 Dresden, Germany
[5] Department fur Geo- und Umweltwissenschaften, Sektion Kristallographie, Ludwig Maximilians Universität, Am Coulombwall 1, D-85748 Garching, München, Germany

E-mail: rajeev@materials.iisc.ernet.in

Received 22 April 2009, in final form 5 June 2009
Published 14 July 2009
Online at stacks.iop.org/JPhysCM/21/326001

Abstract
Temperature-dependent neutron powder diffraction, magnetization and XPS studies were carried out on an optimally Cr-doped $CaRuO_3$, i.e. $CaRu_{0.85}Cr_{0.15}O_3$ (CRC-15). XPS data revealed that Cr exist in 3+ and 6+ oxidation states. The charge dissociation preserves the overall 4+ nominal charge of the Ru site. Although ferromagnetic correlations develop around 100 K, the system exhibits a large coercive field below 50 K. The unit cell volume exhibits negative thermal expansion below 50 K since the lattice expansion due to the magnetostrictive effect outweighs the thermal contraction due to the phonon-driven mechanism.

(Some figures in this article are in colour only in the electronic version)

1. Introduction

The transport and the magnetic properties of narrow itinerant band ruthenium perovskites $SrRuO_3$ (SRO) and $CaRuO_3$ (CRO) have attracted considerable attention over the years. SRO is the only known ferromagnetic conductor in the 4d transition metal oxides with $T_c = 165$ K, and has been the most investigated [1–6]. The Ca analogue, $CaRuO_3$ (CRO), on the other hand, does not exhibit an ordered magnetic state. The itinerant band of these oxides is composed of Ru t_{2g} and O 2p orbitals. The high degree of covalent character of the Ca–O bond as compared to that of the Sr–O bond reduces the width of the itinerant band of CRO, and thereby precludes the onset of an ordered magnetic state in CRO. The ground state of CRO is still under controversy, and the system has been described variously as an exchange-enhanced paramagnetic system [7], showing characteristics of short-range magnetic interactions as a spin glass behaviour [8], on the verge of collective magnetism [4, 9–11], a non-Fermi liquid metal [12], etc. Both SRO and CRO crystallize in the orthorhombic (space group *Pbnm*) $GdFeO_3$-type perovskite structure, characterized by tilted corner-shared RuO_6 octahedra [13–15]. The magnitude of the octahedral deformations and the tilt angle influences the crystal field splitting and the band structure, and hence plays an important role in determining the magnetic properties of SRO [5, 6]. Although there is no satisfactory explanation to describe the true ground state of CRO, it is admitted that the extended 4d orbitals of the Ru ion leads to competing instabilities in the system due to comparable energies for the crystalline fields, spin–orbit coupling, Hund's rule coupling and electron–lattice coupling. The competing instabilities make the system quite susceptible to small perturbations like chemical doping, pressure and magnetic fields. This is evident from the fact that even substitution of ions with no unpaired electrons, such as Ti^{4+} and Sn^{4+} in CRO induces a ferromagnetic state in the system [8, 11]. The coupled nature of the spin–lattice interaction is clearly manifested as the invar effect [16] and freezing of the octahedral tilt angle [17] below the ferromagnetic phase transition of SRO. Of the various types of chemical substitution investigated with regard to their effects

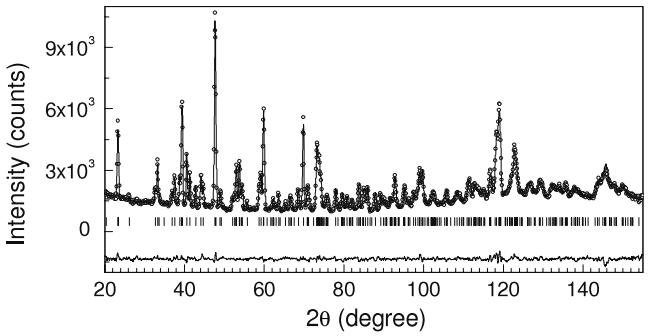

Figure 1. Rietveld plot corresponding to the neutron powder diffraction pattern of $CaRu_{0.85}Cr_{0.15}O_3$ (CRC-15). The filled circles represent the observed data points. The vertical bars indicate the positions of the calculated Bragg peaks.

on the transport and magnetic behaviour of SRO [9, 10, 18, 19] and CRO [8, 9, 19, 20], the Cr substitution is particularly interesting. Cr doping increases the T_c of SRO [10, 18] and induces ferromagnetic interaction in CRO at a temperature as high as 115 K for the optimally doped composition, $CaRu_{0.85}Cr_{0.15}O_3$ (CRC-15) [20]. In this paper, we present the results of XPS, magnetization and structural studies down to 5 K on the optimally Cr-doped $CaRuO_3$. The oxidation states of the doped Cr in the CRO matrix have been investigated to understand the nature of the cationic species responsible for inducing the magnetic exchange interactions in the system. The magneto-elastic coupling effect was investigated using a neutron powder diffraction study and evidence of magneto-elastic coupling was observed below 50 K.

2. Experimental details

A polycrystalline specimen of $CaRu_{0.85}Cr_{0.15}O_3$ (CRC 15) was prepared by the standard solid state reaction of high purity (>99.9%) $CaCO_3$, RuO_2 and Cr_2O_3 chemicals (Alpha Aesar) at 1300 °C for 6 h in air. Neutron powder diffraction data was collected down to 5 K at FRM II (SPODI), Germany, using a wavelength of 1.548 Å. Structural analysis was carried with the Rietveld method using 'FULLPROF' [21]. DC magnetization measurements as a function of temperature and field were carried out with a SQUID magnetometer. XPS data was recorded using Thermo Scientific Multilab 2000 equipment employing Al Kα x-rays. The binding energies were determined within an accuracy of ±0.1 eV. For XPS measurements, the pellet was scratched just before mounting within the sample holder. Since the compound was sufficiently conducting no charging of the sample was noticed.

3. Results and discussion

3.1. Neutron powder diffraction study

The neutron powder diffraction pattern of CRC 15 could be nicely fitted with the orthorhombic structural model (space group *Pbnm*) of the parent compound CRO at all temperatures. The asymmetric unit of the structure consists of one Ca at $(0.5+\delta x_{Ca}, 0.0+\delta y_{Ca}, 0.25)$, one Ru/Cr at (0, 0, 0), one oxygen (O1) at $(0.5+\delta x_{O1}, 0.5+\delta y_{O1}, 0.25)$ and another oxygen (O2) at $(0.25+\delta x_{O2}, 0.25+\delta y_{O2}, 0+\delta z_{O2})$ atomic site, where the various δs represent the refinable parameters. Figure 1 shows the Rietveld plot of the neutron powder diffraction pattern of CRC 15 at 5 K after Rietveld refinement. The refined structural parameters at two representative temperatures, 270 and 5 K, are listed in table 1. For the sake of comparison, we have also listed the structural parameters of CRO at 300 K in the same table. A comparison of the lattice parameters and cell volume of both the systems reveals that the lattice of CRC-15 is significantly shrunk as compared to the parent compound CRO. It may be mentioned that, although the temperature of CRC-15 is 30 K lower than that of CRO, the smaller volume of CRC-15 cannot be attributed primarily to thermal contraction since the difference in the volumes of the two systems is larger than the overall change in the volume of CRC-15 while cooling from 270 to 5 K (see table 1). Since the Shannon ionic radii of Cr^{3+} (0.62 Å, for coordination number 6) is very close to that of Ru^{4+} (0.615 Å) [22], the shrinkage of the lattice on Cr substitution can happen only when some of the elements exist in higher oxidation states. It is shown later that a significant fraction of Cr exists in the 6+ oxidation state (ionic radii = 0.44 Å), which can account for the contraction of the lattice. Although the lattice parameters have decreased on Cr substitution, the table suggests that the positional coordinates of the atoms of CRC-15 and CRO are almost identical, suggesting rigidity of the octahedral tilts in the structure. This finding is in agreement with the recently reported high temperature structural study of CRO in which it has been shown that the octahedral tilts of CRO are very rigid and do not change significantly on heating up to 1300 °C [15]. Table 2 lists the important interatomic distances and bond angles of CRC-15 at 270 and 5 K. ABO_3 perovskites consist of two types of cationic polyhedra centred at the A- and B-sites. In the most symmetric cubic form the A-site is surrounded by 12 equidistant oxygen ions and the B-site by 6 oxygen

Table 1. Structural parameters of CRO and CRC-15. The space group is *Pbnm* (no. 62). The structural data were modelled for Ca and O1 ions occupying the 4*c* position with $z/c = 1/4$, Ru occupies the position 4*b* [0, 0, 0]. Numbers in parentheses give statistical errors in the last significant digit.

Structural parameters	$CaRuO_3$	$CaRu_{0.85}Cr_{0.15}O_3$	
	300 K	270 K	5 K
a (Å)	5.3652(3)	5.3603(1)	5.3489(2)
b (Å)	5.5310(3)	5.4969(2)	5.4976(2)
c (Å)	7.6699(5)	7.6475(2)	7.6367(2)
V (Å^3)	227.61(2)	225.33(1)	224.57(1)
x_{Ca}	0.483(1)	0.4888(9)	0.4868(8)
y_{Ca}	0.0540(6)	0.0502(5)	0.0522(4)
B_{Ca}	0.40(9)	0.72(5)	0.27(5)
$B_{Ru/Cr}$	0.24(4)	0.17(4)	0.06(4)
x_{O1}	0.593(2)	0.5874(5)	0.5883(5)
y_{O1}	0.480(3)	0.4774(5)	0.4760(5)
B_{O1}	0.3(3)	0.55(5)	0.33(4)
x_{O2}	0.203(2)	0.2013(3)	0.2006(3)
y_{O2}	0.293(2)	0.2969(3)	0.2967(3)
z_{O2}	0.049(1)	0.0455(2)	0.0462(2)
B_{O2}	0.1(2)	0.53(3)	0.30(3)

Table 2. Inter atomic distances and bond angles of CRC-15 along with their respective multiplicity at 270 and 5 K.

Distance/angle	5 K	270 K
Ca–O1 (Å)		
×1	2.310(5)	2.306(5)
×1	2.392(4)	2.406(4)
×1	3.106(5)	3.116(5)
×1	3.214(4)	3.193(4)
Ca–O2 (Å)		
×2	2.323(3)	2.329(3)
×2	2.564(4)	2.581(4)
×2	2.668(3)	2.666(3)
×2	3.405(3)	3.392(3)
Ca–Ru/Cr (Å)		
×2	3.126(2)	3.116(2)
×2	3.256(3)	3.242(3)
×2	3.352(4)	3.356(4)
Ru/Cr–O1 (Å)		
×2	1.971(2)	1.973(2)
Ru/Cr–O2 (Å)		
×2	1.984(2)	1.982(2)
×2	1.985(2)	1.987(2)
O1–Ru/Cr–O1 angle (deg)		
×1	180.0(1)	180.0(1)
O1–Ru/Cr–O2 angles (deg)		
×2	89.3(1)	89.4(1)
×2	89.0(1)	89.2(1)
×2	90.7(1)	90.6(1)
×2	91.0(1)	90.8(1)
O2–Ru/Cr–O2 angles (deg)		
×2	90.3(1)	90.4(1)
×2	180.0(1)	180.0(1)
×2	89.7(1)	89.6(1)

ions forming a regular BO_6 octahedra. Octahedral tilts and distortions lead to deformation of these polyhedral units. Of the 12 oxygens that would form the oxygen coordination polyhedron of Ca, four belong to O1 and the remaining eight (four pairs) belong to O2 of the asymmetric unit. Of these, two Ca–O1 type bonds are ∼3.1 and ∼3.2 Å long and one pair of Ca–O2 bond is ∼3.4 Å (see table 2). These four distances are similar to those of Ca–Ru/Cr interatomic distances in the structure (see table 2), and, hence, cannot be ascribed to part of the oxygen coordination polyhedron of Ca. As a result, the highly distorted coordination polyhedron of Ca is constituted of only eight oxygen atoms 2.3–2.7 Å away. In contrary, the six Ru/CrO_6 bond lengths are quite similar (1.97, 1.98 and 1.99 Å), suggesting that, on average, the Ru/CrO_6 polyhedra are nearly regular. This is also obvious from the various O–Ru/Cr–O bond angles that lie close to either 180° or 90°. It is further evident from table 2 that the listed interatomic distances and the bond angles do not vary significantly when cooled from 270 to 5 K.

3.2. X-ray photoelectron spectroscopy study

Figure 2 shows the XPS spectra of the Cr 2p and Ru 3p of CRC-15. Both the $2p_{1/2}$ and $2p_{3/2}$ peaks of Cr 2p states are split into two. Since the kinetic energy of Cr (2p) electrons with Al Kα radiation is ∼910 eV, the mean escape depth is ∼30 Å. Thus the XPS data are obtained from about 70–90 Å

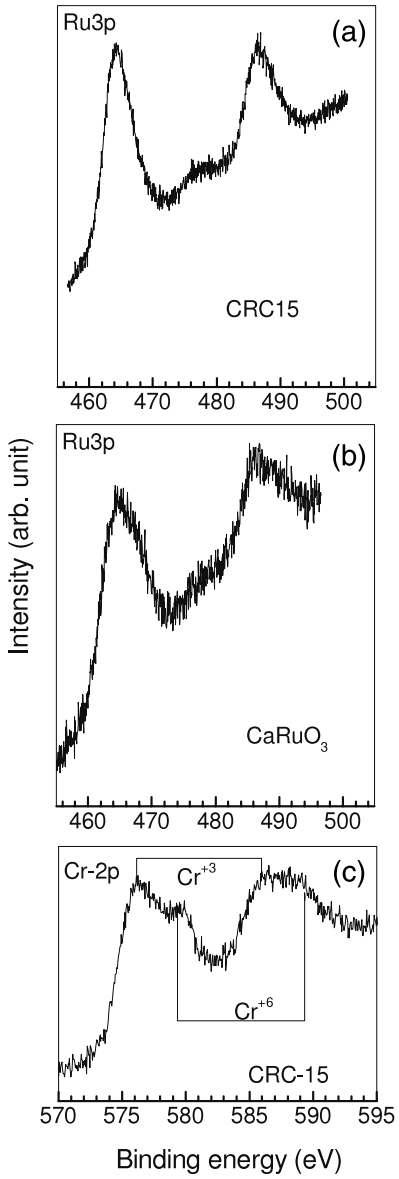

Figure 2. Comparison of the Ru 3p XPS spectra of CRC-15 (a) and $CaRuO_3$ (b) and XPS spectrum of Cr 2p (c).

thickness of the sample, and may be treated as representative of the bulk electronic structure. The doublets occurring at 577 and 579.5 eV in figure 2(c) correspond to 3+ and 6+ oxidation states of Cr. The reproducibility of the data was confirmed by repeating the experiments on a fresh surface of the pellet. Similar mixed valence states of the Cr ion have been reported in $Ce_{2/3}Cr_{1/3}O_{2.1}$ [23]. Assuming that the oxidation states of Cr spilt in CRC-15 so as to maintain the overall 4+ oxidation state of the Ru site, one would expect $Cr^{3+}_{0.15-y}Cr^{6+}_{y} = Cr^{4+}_{0.15}$. This gives $y = 0.05$, that is one-third of the substituted Cr elements should exist in the 6+ oxidation state and two-thirds in the 3+ oxidation state. The intensity ratio of the Cr 2p doublet observed in figure 2 is also very close to 2:1, indicating that the distribution of the oxidation states of Cr preserves the overall 4+ oxidation state of the Ru site. In this scenario, one would not expect the Ru to exhibit an oxidation state other than 4+. The similarity of the Ru 3p XPS spectra of pure CRO

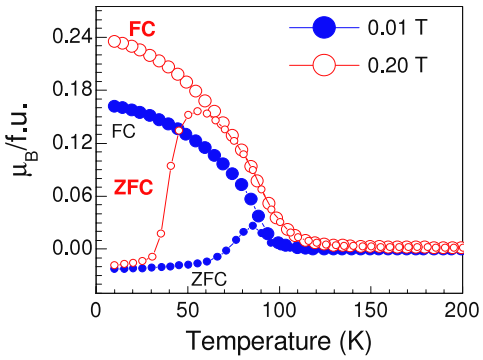

Figure 3. Temperature dependence of zero-field-cooled (ZFC) and field-cooled (FC) magnetization of $CaRu_{0.85}Cr_{0.15}O_3$ at 0.01 and 0.2 T fields.

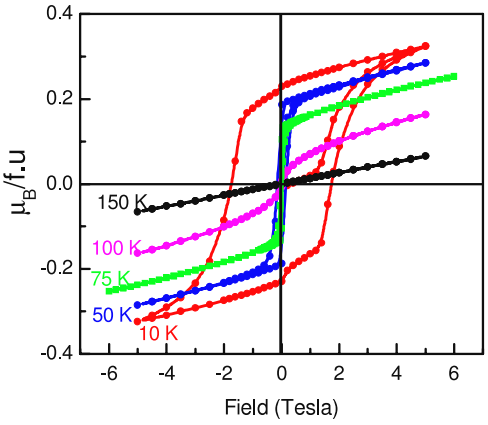

Figure 4. Magnetic hysteresis of $CaRu_{0.85}Cr_{0.15}O_3$ at four different temperatures.

and CRC-15 further suggests that the oxidation state of Ru in CRO (4+) is the same as in CRC-15 (figure 2(a)). It is likely that the local coordination of the Cr^{3+} and the Cr^{6+} can be different leading to development of local random strain in the system. In view of the delicate balance of competing energies of the various degrees of freedom in CRO, such strains can as well be a factor promoting ferromagnetic correlations in the system. This view seems to be further supported by the fact that even by substitution of nonmagnetic ions such as Ti^{4+} [8] and Sn^{4+} [11], which would contribute to local strain due to ionic size difference, ferromagnetic correlations can be stabilized in CRO.

3.3. Magnetization study

Figure 3 shows the zero-field-cooled (ZFC) and field-cooled (FC) magnetization as a function of temperature of CRC-15 at two different fields 0.01 and 0.2 T. The ZFC curves correspond to warming the sample while the field was applied. At a field of 0.01 T, ZFC and FC branches separate below ∼110 K showing evidence of irreversibility. At a relatively higher field of 0.2 T, the irreversibility sets in at a lower temperature. The magnitude of the peak of the ZFC branch, and the saturation magnetization at low temperatures of the FC branch increases with increasing field strength. Similar results have been reported earlier by Felner *et al* [24] for different cationic substitutions. Figure 4 shows the magnetization hysteresis curves at five representative temperatures, 10, 50, 75, 100 and 150 K. At 150 K the curve is linear, suggesting a paramagnetic state. Nonlinearity, corresponding to the setting in of ferromagnetic correlation, is observed at 100 K, though a well-defined but narrow hysteresis loop develops at 75 K and below, with the remanent magnetization increasing slowly upon cooling. A notable feature, however, is a drastic increase in the coercive field at 10 K, suggesting enhanced rigidity of the domain walls at this temperature. This may be attributed to increase of the strain fields at low temperature which enhances the domain pinning tendency. The saturation magnetization at 10 K is ∼0.25 μ_B/f.u. which is nearly one-fourth of the value reported for SRO [4].

3.4. Thermal expansion behaviour

Figure 5 depicts the variation of orthorhombic lattice parameters of CRC-15 as a function of temperature in the

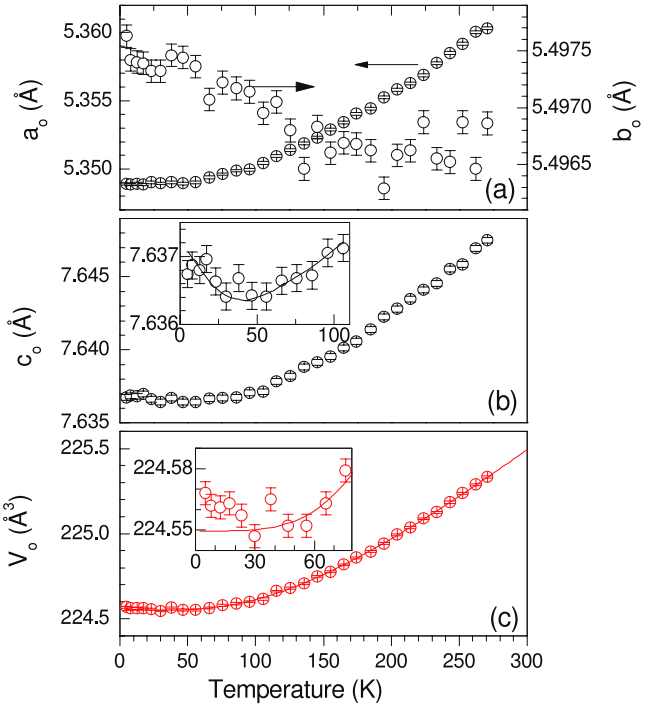

Figure 5. Temperature variation of the orthorhombic lattice parameters and unit cell volume of $CaRu_{0.85}Cr_{0.15}O_3$. The continuous line in the bottom panel of the figure is the best fit curve represented by equations (1) in the text. The inset in (c) shows evidence of negative thermal expansion behaviour below 50 K. The continuous line in inset (b) is a guide to the eye.

range 5–270 K. It may be remarked that the quality of the Rietveld fit to the neutron diffraction pattern at 5 K was the same as it was with the data at 270 K, indicating that the magnetic contribution to the intensity of the Bragg peaks in the ferromagnetic state of the system is extremely weak. It is evident from figure 5 that, while the lattice contracts in the *a* and *c* crystallographic directions on cooling, it expands, though marginally, in the *b* direction. SRO, on the other hand, exhibits a decrease of all three lattice parameters (*a*, *b* and *c*) on cooling [16]. The unit cell volume (*V*) follows the trend exhibited by the *a* and *c* parameters. The data

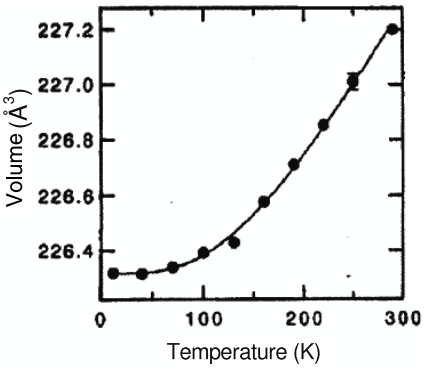

Figure 6. Temperature variation of cell volume of $CaRuO_3$. Reproduced with permission from [16]. Copyright 1996 by the American Physical Society.

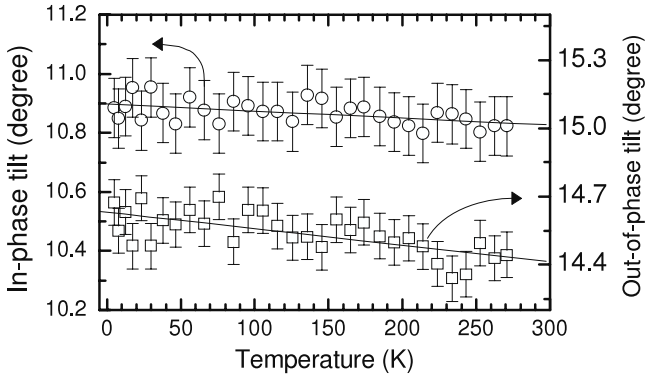

Figure 7. Variation of the in-phase and out-of-phase octahedral tilt angle of $CaRu_{0.85}Cr_{0.15}O_3$ with temperature (see the text).

corresponding to the temperature dependence of volume was fitted with an optimized Debye–Grüneisen function. Using the Debye model for the lattice specific heat, the contribution to thermal expansion by anharmonic parts of the lattice vibration is given by the equation [16]

$$V \cong V(0) + \frac{9\gamma N k_B}{B} T \left(\frac{T}{\Theta_D}\right)^3 \int_0^{\Theta_D/T} \frac{x^3}{e^x - 1}\,dx \quad (1)$$

where $V(0)$, Θ_D, γ and B represent the volume at 0 K, the Debye temperature, the Grüneisen parameter and the bulk modulus, respectively. γ and B have been combined in a single refinable parameter $C(=9\gamma N k_B/B)$. The best fitting curve, shown as a continuous line through the data points in figure 5(c), was obtained with the parameters $V(0) = 224.54$ Å^3, $\Theta_D = 560$ K and $C = 0.011$ Å^3 K^{-1}. It may be remarked that a similar analysis has been done for CRO and SRO in [16]. The constants obtained by us for CRC-15 are very close to the corresponding values reported for pure CRO ($V(0) = 226.3$ Å^3, $\Theta_D = 542$ K and $C = 0.019$ Å^3 K^{-1}) [16]. A careful look at the data points revealed a weak but systematic increase of the observed volume from the fitted curve (see the inset of figure 5(c)). This particular trend was found to have a dominant contribution from the c parameter of the orthorhombic lattice as can be seen from the inset of figure 5(b). Since the Debye–Grüneisen equation predicts the minimum saturated unit cell volume $V(0)$ of the compound at low temperatures, it can in no way explain the systematic increase in the volume below 50 K. For the sake of comparison, the temperature dependence of the cell volume of CRO, as reported in [16], is shown in figure 6. Although the data points are comparatively less in this figure as compared to figure 5(c), the first two data points below 50 K seem to suggest that there is no negative expansion in the low temperature regime of CRO. In view of this, the small negative expansion in CRC-15 can be attributed to a new physical phenomenon. It is likely that the expansion in volume below 50 K is due to magnetostrictive effects similar to what has been reported for SRO [16]. In contrast to the present case, the magnetostrictive effect is quite pronounced in pure SRO leading to the invar effect below 115 K due to compensating effects of the decrease in volume on cooling due to normal phonon-driven processes and increase in the volume due to magnetostriction. In the present case, since the magnetostrictive effect appears below 50 K, i.e. in the temperature region where phonon-driven volume change is nearly zero, the increase in the volume due to the magnetostriction effect results in overall negative expansion.

3.5. Temperature dependence of structural distortion

Dabrowski *et al* [17] have reported that the invar effect in SRO is related to the freezing of the RuO_6 octahedral tilt below the ferromagnetic transition temperature. Following Glazer [25], structural distortion in perovskite compounds is commonly described in terms of tilt of the anion octahedra about the three tetrad axes of the octahedra. These angles are primarily determined using the position of oxygen atoms in the structure. The orthorhombic structure under consideration corresponds to Glazer's tilt notation $a^-a^-c^+$; the equality of the two out-of-phase tilts about the two pseudocubic directions, [100] and [010], can be described as a composite out-of-phase tilt about the [110] pseudocubic direction. The magnitudes of the in-phase tilt (ψ) about [001] and the anti-phase tilt (φ) about [110] were obtained from the displacements of the O2 atoms from (0.25, 0.25, 0) to $(0.25 - u, 0.25 + v, w)$ using the expressions: $\tan\psi = 2(u + v)$ and $\tan\varphi = 4\sqrt{2}w$ [15]. It is evident from figure 7 that the changes in both the tilt angles are negligible (less than 0.1° for the in-phase tilt and less than 0.2° for the out-of-phase tilt) in the entire temperature range. This feature is consistent with the rigidity of the octahedral tilts mentioned above for the parent compound $CaRuO_3$ [15]. Because of the small change in the overall magnitude of the tilt, it is not possible to comment on the possible coupling of octahedral tilt and negative lattice expansion in CRC-15. The temperature variation of five different types of Ca–O bonds discussed above, forming the eight-coordination oxygen polyhedron around the Ca, and the three types of Ru/Cr–O bonds forming the octahedra is shown in figure 8. Similar to the tilt angles mentioned above, the interatomic distances are also almost unaffected by temperature. Further, it is interesting to note that, although the overall symmetry of the structure is orthorhombic, the Ru/Cr–O_6 bond lengths suggest that the

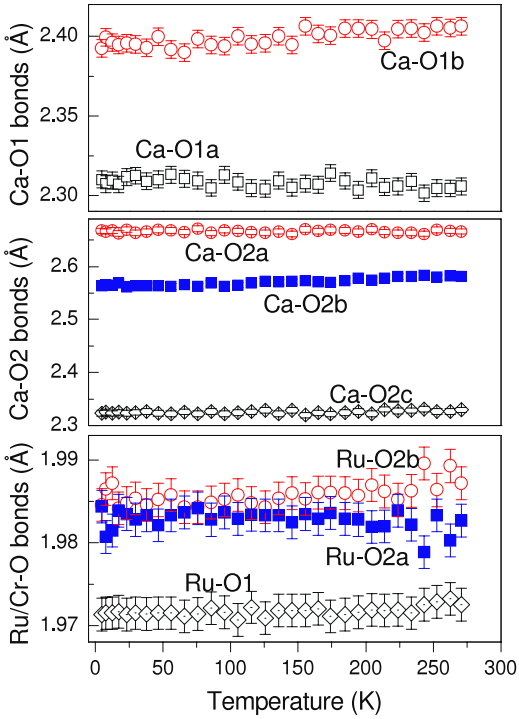

Figure 8. Variation of different bond lengths of $CaRu_{0.85}Cr_{0.15}O_3$ with temperature.

octahedra is weakly tetragonally distorted with four oxygens at ∼1.985 Å and two at ∼1.97 Å. In view of the insignificant variation of the different bond lengths across the temperature, and also the scatter of the data points, it was not possible to correlate the weak negative expansion in volume with any of the bonds discussed above. The main contribution to the trend in the volume at low temperature, as already mentioned above, comes from the *c* parameter.

4. Conclusions

In conclusion, detailed temperature dependent magnetization and structural studies on $CaRu_{0.85}Cr_{0.15}O_3$ have revealed that ferromagnetic correlations build up gradually on cooling the system below 110 K. Ferromagnetic hysteresis can be seen at 75 K and below, and the system exhibits an anomalous increase in coercivity at 10 K and negative thermal expansion behaviour below 50 K, presumably because the expansion due to the magnetostrictive effect outweighs the contraction due to the phonon-driven process. The Cr ions in the specimen are present as Cr^{3+}, a high spin ($t_{2g}^3e_g^0$) $3d^3$ cation and Cr^{6+} (d^0 cation) at room temperature. The charge splitting of the doped Cr seems to preserve the nominal 4+ charge of the Ru site. Since the Cr^{6+} ions have no d-electrons they would not participate in the exchange process with Ru^{4+}. In view of this, the exchange interaction between the host and guest ions, contributing to the development of ferromagnetic correlations in the system, can only be of the type Cr^{3+}–O–Ru^{4+}. Further, though the Cr^{6+} ions would not participate in the magnetic exchange, their significantly smaller ionic radii as compared to Cr^{3+} and Ru^{4+} ions, is likely to induce significant local strain in the system. In view of the presence of competing instabilities in CRO, such a localized strain field can act as a perturbing field to promote the ferromagnetic state, in addition to the Cr^{3+}–O–Ru^{4+} exchange that induces a net ferromagnetic correlation between the Ru^{4+} ions [20].

References

[1] Callaghan A, Moeller C W and Ward R 1966 *Inorg. Chem.* **5** 1572
[2] Longo J M, Raccah P M and Goodenough J B 1968 *J. Appl. Phys.* **39** 1327
[3] Singh D J 1996 *J. Appl. Phys.* **79** 4818
[4] Cao G, McCall S, Shepard M, Crow J E and Guertin R P 1997 *Phys. Rev.* B **56** 321
[5] Mazin I I and Singh D J 1997 *Phys. Rev.* B **56** 2556
[6] Mazin I I and Singh D J 1997 *Phys. Rev. Lett.* **79** 733
[7] Gibb T C, Greatrex R G, Greenwood N N and Kaspi P 1973 *J. Chem. Soc. Dalton Trans.* **1973** 1253
[8] Felner I, Asaf U, Nowik I and Bradaric I 2002 *Phys. Rev.* B **66** 054418
[9] Cao G, McCall S, Bolivar J, Shepard M, Freibert F, Henning P, Crow J E and Yuen T 1996 *Phys. Rev.* B **54** 15144
[10] Pi L, Maignan A, Retoux R and Raveau B 2002 *J. Phys.: Condens. Matter* **14** 7391
[11] He T and Cava R J 2001 *J. Phys.: Condens. Matter* **13** 8347
[12] Klein L, Antognazza L, Geballe T H, Beasley M R and Kapitulnik A 1999 *Phys. Rev.* B **60** 1448
[13] Bouchard R J and Gillson J L 1972 *Mater. Res. Bull.* **7** 873
[14] Geller S and Wood E A 1956 *Acta Crystallogr.* **9** 563
[15] Ranjan R, Senyshyn A, Vashook V, Niewa R, Boysen H and Frey F 2007 *Appl. Phys. Lett.* **90** 251913
[16] Kiyama T, Yoshimura K, Kosuge K, Ikeda Y and Bando Y 1996 *Phys. Rev.* B **54** R756
[17] Dabrowski B, Avdeev M, Chmaissem O, Kolesnik S, Klamut P W, Maxwell M and Jorgensen J D 2005 *Phys. Rev.* B **71** 104411
[18] Williams A J, Gillies A, Attfield J P, Heymann G, Huppertz H, Martinez-Lope M J and Alonso J A 2006 *Phys. Rev.* B **73** 104409
[19] Durairaj V, Chikara S, Lin X N, Douglass A, Cao G, Schlottmann P and Guertin R P 2006 *Phys. Rev.* B **73** 214414
[20] Maignan A, Raveau B, Hardy V, Barrier N and Retoux R 2006 *Phys. Rev.* B **74** 024410
[21] Rodrigues-Carvajal J 2000 *FULLPROF 2000. A Rietveld Refinement and Pattern Matching Analysis Program* Laboratoire Leon Brillouin (CEA-CNRS) France
[22] Shannon R D 1976 *Acta Crystallogr.* A **32** 751
[23] Singh P, Hegde M S and Goplakrishnan J 2008 *Chem. Mater.* **20** 7268
[24] Felner I, Nowik I, Bradaric I and Gospodinov M 2000 *Phys. Rev.* B **60** 1448
[25] Glazer A M 1975 *Acta Crystallogr.* A **31** 756